Monthly Notices
of the
ROYAL ASTRONOMICAL SOCIETY

MNRAS **492,** 3803–3815 (2020)
Advance Access publication 2020 January 10

doi:10.1093/mnras/staa049

Standard siren speeds: improving velocities in gravitational-wave measurements of H_0

Cullan Howlett ★ and Tamara M. Davis

School of Mathematics and Physics, The University of Queensland, Brisbane, QLD 4072, Australia

Accepted 2020 January 6. Received 2020 January 6; in original form 2019 August 30

ABSTRACT

We re-analyse data from the gravitational-wave event GW170817 and its host galaxy NGC 4993 to demonstrate the importance of accurate total and peculiar velocities when measuring the Hubble constant using this nearby standard siren. We show that a number of reasonable choices can be made to estimate the velocities for this event, but that systematic differences remain between these measurements depending on the data used. This leads to significant changes in the Hubble constant inferred from GW170817. We present Bayesian model averaging as one way to account for these differences, and obtain $H_0 = 66.8^{+13.4}_{-9.2}$ km s^{-1} Mpc^{-1}. Adding additional information on the viewing angle from high-resolution imaging of the radio counterpart refines this to $H_0 = 64.8^{+7.3}_{-7.2}$ km s^{-1} Mpc^{-1}. During this analysis, we also present an alternative Bayesian model for the posterior on H_0 from standard sirens that works more closely with observed quantities from redshift and peculiar velocity surveys. Our results more accurately capture the true uncertainty on the total and peculiar velocities of NGC 4993 and show that exploring how well different data sets characterize galaxy groups and the velocity field in the local Universe could improve this measurement further. These considerations impact any low-redshift distance measurement, and the improvements we suggest here can also be applied to standard candles like Type Ia supernovae. GW170817 is particularly sensitive to peculiar velocity uncertainties because it is so close. For future standard siren measurements, the importance of this error will decrease as (i) we will measure more distant standard sirens and (ii) the random direction of peculiar velocities will average out with more detections.

Key words: methods: statistical – galaxies: distances and redshifts – galaxies: individual: NGC 4993 – cosmological parameters.

1 INTRODUCTION

On 2017 August 17, the Advanced LIGO (LIGO Scientific Collaboration 2015) and Advanced Virgo (Acernese et al. 2015) detectors observed gravitational waves originating from event GW170817. Modelling of this signal later identified this event as a result of the merger of two compact neutron stars (Abbott et al. 2017a, 2019). In the short time after that, electromagnetic counterparts were detected across a number of wavelengths (Abbott et al. 2017c) resulting in the first multimessenger detection of a gravitational wave.

The presence of the electromagnetic counterparts gave a precise determination (with probability of chance association $P <$ 0.004 per cent; Abbott et al. 2017b) that the host of the gravitational wave was NGC 4993, a low-redshift lenticular galaxy. The combination of gravitational wave and host identification then allowed for the first ever 'standard siren' measurement of the Hubble constant, H_0, analogous to methods using 'standard candles' (Type Ia supernovae – SNe Ia; Cepheid variable stars, etc.) and 'standard rulers' (e.g. Baryon Acoustic Oscillations – BAOs; the cosmic microwave background – CMB). This determination of the Hubble constant was made possible through the combination of cosmological luminosity distance inferred from the gravitational-wave signal, combined with the observed total and peculiar velocities of NGC 4993. The luminosity distance inferred from the gravitational wave is consistent with independent measurements of the distance to NGC 4993 (e.g. Hjorth et al. 2017; Im et al. 2017; Cantiello et al. 2018). It is worth noting that in cosmological terms, standard sirens and candles are very similar; both measure the luminosity distance through calibration of an astrophysical signal, which in the case of standard sirens is the frequency and rate of change of frequency of the gravitational wave. This can be compared to standard rulers, which measure a different cosmological quantity, the angular diameter distance.

The Hubble constant is one of the fundamental constants describing our cosmological model. It describes how fast the Universe

★ E-mail: c.howlett@uq.edu.au

© 2020 The Author(s)
Published by Oxford University Press on behalf of the Royal Astronomical Society

Downloaded from https://academic.oup.com/mnras/article-abstract/492/3/3803/5700291 by University of Queensland user on 20 April 2020

is expanding, and how fast objects are receding from each other. Precise determination of this constant has been one of the foremost goals of cosmology since its discovery, with the majority of measurements using either standard candles or standard rulers. In recent years, tensions have arisen between measurements from these two methods. Results from a combination of *Planck* CMB and various BAO measurements prefer $H_0 = 67.66 \pm 0.42\,\mathrm{km\,s^{-1}\,Mpc^{-1}}$ (Planck Collaboration VI 2018); however, this requires assuming a lambda cold dark matter (ΛCDM) cosmological model to extrapolate the constraints from high redshift. Results using the local distance ladder (SNe anchored using Cepheids and local geometric distances) prefer $H_0 = 74.03 \pm 1.42\,\mathrm{km\,s^{-1}\,Mpc^{-1}}$ (Riess et al. 2019).[1] The tension between these two is currently at the level of $\sim 4.5\sigma$ and hints at the presence of unknown systematics or new fundamental physics. It seems unlikely that this will be resolved over the coming years without additional, independent measurements. Standard sirens using gravitational waves present the exciting prospect of such a measurement, and may identify a way to resolve the current tension.

Standard sirens are one of the cleanest distance measurements available, but they are not without their own sources of uncertainty, both statistical and systematic. Especially in the infancy of this technique, with few measurements available, these could cause biases in the recovered constraints on the Hubble constant. The potential source of systematic uncertainty we concentrate on in this paper is the influence of peculiar velocities. Peculiar velocities have long been known to potentially bias measurements of H_0, particularly if the sources are nearby (e.g. Dressler et al. 1987; Sandage & Tammann 1990; Tonry et al. 2000; Tully et al. 2008). We begin by summarizing how peculiar velocities impact H_0 estimates in general, and then consider the specifics of the peculiar velocity estimates of GW170817's host, NGC 4993.

With determination of the host galaxy and a measurement of the luminosity distance d_L, we can infer the Hubble constant via

$$(1 + z_\mathrm{obs}) = (1 + \bar{z}(d_\mathrm{L}, H_0, z_\mathrm{obs}))\left(1 + z_\mathrm{p}^\mathrm{obj}\right)\left(1 + z_\mathrm{p}^\mathrm{Sun}\right), \tag{1}$$

where z_obs is the observed redshift and $z_\mathrm{p}^\mathrm{obj}$ is the peculiar redshift that arises from the peculiar velocity of the observed object. $\bar{z}(d_\mathrm{L}, H_0, z_\mathrm{obs})$ is the cosmological redshift of the object, which can be computed given a choice of the Hubble constant and an inference of the luminosity distance. $z_\mathrm{p}^\mathrm{Sun}$ is an additional redshift arising from our Sun's motion with respect to the comoving frame, typically calculated using the CMB dipole. For reference, the relationship between peculiar redshift (of either an observed object or our Solar system) and velocity is given by

$$1 + z = \sqrt{\frac{1 + v/c}{1 - v/c}} \approx 1 + v/c, \tag{2}$$

where c is the speed of light and the approximation holds as long as $v_\mathrm{p} \ll c$ (Davis et al. 2019). Note that this relationship is only appropriate for objects moving within their local inertial frame and so is not appropriate for converting the cosmological redshift $\bar{z}$ to a velocity (Davis & Lineweaver 2004).

It is common to see equation (1) computed using a number of approximations, where first the CMB dipole is used to convert the observed redshift to the redshift we would have observed if we had no peculiar velocity and were comoving observers (in the CMB frame) using the approximation $z_\mathrm{cmb} = z_\mathrm{obs} - z_\mathrm{p}^\mathrm{Sun}$ and then the Hubble constant is inferred using

$$cz_\mathrm{cmb} = v_\mathrm{p}^\mathrm{obj} + H_0^\mathrm{approx} d_\mathrm{L}/(1 + z_\mathrm{cmb}). \tag{3}$$

However, we will tacitly avoid such approximations in this work and demonstrate that they are unnecessary (and inadequate) for inferring the Hubble constant from standard sirens. It is also common to use redshifts and velocities interchangeably, which leads to potential confusion/mistakes. For clarity, we provide in Table 1 a list of definitions for the various terms used in this work.

Regardless of the approximations used, constraining the Hubble constant using gravitational waves (or indeed any local distance measurement) requires knowledge of the observed object's total and peculiar velocities. There are a number of methods to estimate these in combination. First, the total velocity of the host can be measured spectroscopically and combined with a measurement of the peculiar velocity of the host. However, in this case, the total and peculiar velocities of the host galaxy are influenced by its motion within its Local Group or cluster, which includes non-linear effects from growth of structure and/or virialized motions that may be hard to account for in the peculiar velocity estimate. The peculiar velocity for a single object is also subject to considerable statistical error. It is often preferable, as was done in Abbott et al. (2017b), to use instead the total and peculiar velocity of the group to which the object belongs such that non-linear motions are 'smoothed-out' and the uncertainty in the peculiar velocity reduced. In this case, there still remains a choice of how to compute which galaxies belong to the same group as the host, and how to obtain the peculiar velocity of the group.

In terms of estimating the group peculiar velocity, there are two approaches commonly adopted. The first is to use a 'peculiar velocity survey'; a catalogue of measured peculiar velocities estimated for objects with secondary distance measurements (more detail on these is given in Section 3). Different interpolation methods can then be applied to this catalogue to estimate the peculiar velocity at the location of the group. In this case, however, it is worth noting that peculiar velocity is not actually the directly observed quantity from peculiar velocity surveys (it is the change in magnitude or size caused by the underlying peculiar velocity) and hence the uncertainties in the measured peculiar velocities are not typically Gaussian distributed (unless an approximate estimator is used; Watkins & Feldman 2015). The second method is to use measurements of the density field from galaxy redshift surveys combined with theoretical (linear or quasi-linear) predictions for the relationship between the density and velocity fields to reconstruct the gravitational infall on to large-scale structures. Overall, this is to say that there are a number of choices one can make for how to estimate the joint total and peculiar velocities of the observed object. Should we use the properties of the host *or* its group? If the latter, which group catalogue should we believe? Should the peculiar velocity be estimated using peculiar velocity surveys or reconstructions?

Abbott et al. (2017b) present one such combination of methods to estimate both the CMB-frame redshift (which they treat as the total velocity) and peculiar velocity of the group containing NGC 4993. These are given values of $cz_\mathrm{cmb} = 3327 \pm 72\,\mathrm{km\,s^{-1}}$ and $v_\mathrm{p}^\mathrm{host} = 310 \pm 150\,\mathrm{km\,s^{-1}}$, respectively, in their canonical analysis. Using these values and equation (3) they obtain the first ever measurement of H_0 using standard sirens, $H_0 = 70.0^{+12.0}_{-8.0}\,\mathrm{km\,s^{-1}\,Mpc^{-1}}$. This was improved upon by Hotokezaka et al. (2019) to $H_0 =$

[1] However, very recent results suggest that changing the Cepheid anchor to TRGB stars can cause significant shifts in the preferred Hubble constant (Freedman et al. 2019).

Downloaded from https://academic.oup.com/mnras/article-abstract/492/3/3803/5700291 by University of Queensland user on 20 April 2020

Table 1. Definitions of redshifts and their corresponding velocities used in this work, the relationship between them, and the physical description of their origin.

Redshifts		Velocities		Description
Name	Symbol	Name	Symbol	
Observed redshift	$z_{\rm obs}$	Total velocity	$v_{\rm t}$	The redshift/velocity of an object as measured by us in the heliocentric (Sun-centred) frame, i.e. after correcting for the rotation of the Earth, and its motion around the Sun, *but without* any corrections for the Sun's motion relative to the CMB dipole, or correction for the observed object's motion. Equal to the combined contributions from the Sun's peculiar, object's peculiar, and recession velocities, i.e. the product of the relevant $(1+z)$ factors, equation (1).
Cosmological redshift	$\bar{z}$	Recession velocity	$v_{\rm r}$	The redshift/velocity of the observed object due to the expansion of the Universe.
Object's peculiar redshift	$z_{\rm p}^{\rm obj}$	Object's peculiar velocity	$v_{\rm p}^{\rm obj}$	The component of the redshift/velocity of the observed object due to its motion towards/away from us, in departure from the expansion of the universe. The peculiar redshift and peculiar velocity are related by equation (2).
Sun's peculiar redshift	$z_{\rm p}^{\rm Sun}$	Sun's peculiar velocity	$v_{\rm p}^{\rm Sun}$	The component of the redshift/velocity of an object due to the motion of *our* Solar system in the direction of the observed object, relative to the CMB rest frame. This is typically inferred from measurements of the amplitude and direction of the CMB dipole. The Sun's peculiar redshift and peculiar velocity are related by equation (2).
CMB-frame redshift	$z_{\rm cmb}$	CMB-frame velocity	$v_{\rm cmb}$	The redshift/velocity of the object after correcting for our Solar system's peculiar motion with respect to the CMB dipole. This should represent the redshift with us in the comoving frame, but may still have contributions from the observed galaxy's/host's peculiar velocity. This should be computed using $(1+z_{\rm cmb}) = \frac{(1+z_{\rm obs})}{(1+z_{\rm p}^{\rm Sun})}$ but is often approximated.

$68.9^{+4.7}_{-4.6}\,{\rm km\,s^{-1}\,Mpc^{-1}}$ using very long baseline interferometer (VLBI) measurements of the centroid motion and afterglow light curve of the jet associated with GW170817, which substantially improves the degeneracy between the luminosity distance and observing angle.

In this work, we will demonstrate that for the sole case of GW170817 and its host NGC 4993 there are a number of alternative methods that could be used to obtain the total and peculiar velocities required for the standard siren determination of H_0. Although this is not an exhaustive list (for instance, we focus on peculiar velocity surveys, and do not consider the range of reconstructions one could also use), among these cases we identify systematic differences that are larger than the uncertainties commonly used for these measurements suggest. These differences translate into a range of Hubble constants; again wider than the uncertainty on H_0 from Abbott et al. (2017b) or Hotokezaka et al. (2019). Although the error is currently large, studies (e.g. Chen, Fishbach & Holz 2018; Shafieloo, Keeley & Linder 2018; Mortlock et al. 2019; Zhang et al. 2019) show that with only a handful of similar cases, we could obtain constraints on H_0 comparable to those from standard candles or rulers. Whilst the impact of peculiar velocity uncertainties may reduce as more objects are detected at larger distances, it will be some time before peculiar velocities become a sub-dominant source of uncertainty. Hence, understanding and accounting for systematic differences in our estimates of the host's velocity is important if standard sirens are to be considered a reliable way to measure H_0 in the near future.

It is worth noting that this problem is most prevalent for current standard siren measurements with identifiable hosts. In the case where the true host is unknown and marginalized over (e.g. Fishbach et al. 2019; Soares-Santos et al. 2019), the impact of peculiar velocity errors will be smaller, both because the uncertainty on H_0 will be larger and because the peculiar velocities should be randomly oriented and will partially cancel out (although one would ideally hope for a small localization area, which would mean the velocities will be correlated and cancel out less effectively). Even at nearby distances with electromagnetic counterparts, the error in peculiar velocities should partially cancel out as more standard sirens are detected. However, we will need hundreds of standard sirens before this is effective and there could still be a residual bias even after many hundreds have been averaged if the peculiar velocity errors are asymmetric or systematic. These errors would also impact supernova measurements but as SNe are typically at higher observed redshift the impact is smaller. Cosmological studies usually reject any SNe closer than $z_{\rm obs} < 0.02$ which is where the typical peculiar velocity should contribute less than 5 per cent uncertainty to the total velocity.

We order this work as follows: In Section 2, we present a number of determinations for the group total velocity (or rather the group observed redshift) of NGC 4993. In Section 3, we do the same for the peculiar velocity/redshift. In both cases, we identify a number of reasonable choices that give significantly different results. In Section 4, we show how these choices change the inferred Hubble constant, but also offer a way in which such systematic differences could be folded into the marginalized constraints. We conclude in Section 5. Where necessary, or unless otherwise stated, we assume a flat ΛCDM cosmology with $\Omega_{\rm m} = 0.3$. Given the low redshift of the sample, we do not expect changing this to affect our results (in particular any distance calculations), and any distances used herein that may affect the extraction or interpretation of the Hubble constant are given independent of its value (i.e. in units of h^{-1} Mpc).

2 ESTIMATES OF THE GROUP OBSERVED REDSHIFT

The galaxy NGC 4993 has been identified as belonging to a larger group of galaxies in a number of different studies. The total and peculiar velocities of the group can be used in place of the individual galaxy in order to reduce the effects of non-linearities and internal peculiar motions and to improve the precision with which the peculiar velocity is known. The argument is as follows: the size of the cluster is small enough that the distance to the

Downloaded from https://academic.oup.com/mnras/article-abstract/492/3/3803/5700291 by University of Queensland user on 20 April 2020

cluster is approximately the distance to the galaxy that hosted the gravitational wave. For an object such as NGC 4993 (with CMB-frame redshift $cz_{\rm cmb} = 3228 \pm 15\,{\rm km\,s^{-1}}$) the peculiar motion of the galaxy within its group or cluster could easily be as much as 20 per cent of the CMB-frame velocity. Hence, the internal peculiar motion is expected to give a larger error than the error due to using the centre of the cluster as the distance (see Table 2 for estimates of such a distance for NGC 4993). Similarly, using the redshift of the cluster is closer to the cosmological redshift than a galaxy within the cluster will be.

A second benefit of using the velocities for the group is that the peculiar velocity of the group can be measured with higher precision than for an individual object. For peculiar velocities estimated using a peculiar velocity catalogue, the measurements for individual group members can be averaged over. For estimates obtained from reconstructions, the density field can be smoothed on scales comparable to the group size, such that linear theory can be more reliably used to estimate the velocities without need for additional uncertainties to account for non-linearities.

As a caveat, one downside of using the group velocities is the potential to mistake the host as a member of a group when it is not. Ensuring the group catalogues used to identify the host's group are robust is critical in obtaining reliable H_0 estimates. Comparing or marginalizing over different group catalogues reduces the potential for these 'catastrophic errors' somewhat, but may not mitigate against it entirely because many group catalogues use overlapping data or similar algorithms.

Abbott et al. (2017b) used the High Density Catalogue (HDC) of Crook et al. (2007, 2008) (which contains five members including NGC 4993) to estimate a CMB-frame redshift of the group, after correcting for our own motion with respect to the CMB, of $cz_{\rm cmb} = 3327 \pm 72\,{\rm km\,s^{-1}}$. The corresponding observed redshift, without correction for our motion, taken directly from the group catalogue is $cz_{\rm obs} = 3016 \pm 72\,{\rm km\,s^{-1}}$. In both cases, the redshift has been multiplied by the speed of light to give units of ${\rm km\,s^{-1}}$, but we emphasize that these should not be treated as the total velocity and CMB-frame velocity (because $v_{\rm t} \neq cz_{\rm obs}$). However, differences in the choice of data and algorithm used to construct the group catalogue can lead to differences in the group observed redshift larger than the uncertainty quoted above. Table 2 presents a number of estimates for the group observed redshift, with and without conversion to the CMB frame, of NGC 4993. There is significant overlap between the data used to construct these groups, and many of these rely on data from the 2MASS Redshift (Huchra et al. 2012), 6-degree Field Galaxy Redshift (Jones et al. 2009), and Sloan Digital Sky (York et al. 2000) surveys. However, they differ in the clustering algorithms used, their treatment of the various selection effects in the data including if any fainter objects are included, and how the group properties including mean velocities and velocity dispersions are calculated. This is reflected in the variation in the quantities presented in Table 2 even for group catalogues that are built from similar data.

Some of the estimates of the observed redshift of the group containing NGC 4993 in Table 2 can be identified as spurious. For instance the estimate using the Crook et al. (2008) Low Density Catalogue (LDC) gives a value significantly lower than other sources. As pointed out in Hjorth et al. (2017), inspection of the galaxies in the Crook et al. (2008) LDC group shows that NGC 4993 is only peripherally associated with this structure, as can also be inferred from the large distance between NGC 4993 and the group centre given in Table 2. Hjorth et al. (2017) provide their own estimate of the group total velocity using a refined version of the

Table 2. Properties of groups containing NGC 4993 from various group catalogues. The first row is the properties of NGC 4993 itself. The second row contains the properties used in the original Abbott et al. (2017b) analysis. For each group we list the group identifier, the number of members N, the mean observed redshift, and CMB-frame redshift (both multiplied by the speed of light to give units of ${\rm km\,s^{-1}}$) with error computed from the velocity dispersion divided by the square root of the number of members. We then compute the 3D (not projected) distance from NGC 4993 to the centre of the group assuming our fiducial cosmology to convert to Cartesian coordinates. We additionally identify how many members in the group have distance measurements in the Cosmic-Flows III compilation $N(v_{\rm p})$, and compute the mean log-distance ratio and peculiar velocity. See Section 3 for a description of how these are computed. Each of the group catalogues can be obtained from its respective reference, except the catalogue based on the 6-degree Field Galaxy Redshift Survey (6dFGRS), which was obtained from Merson, Heath Jones & Colless (private communication). Kourkchi & Tully (2017) (Trimmed) indicates we have removed the galaxies from this group that were identified by Hjorth et al. (2017) as only being loosely associated with the group.

Reference	Group name	N	Observed redshift $cz_{\rm obs}$ (${\rm km\,s^{-1}}$)	CMB-frame redshift $cz_{\rm cmb}$ (${\rm km\,s^{-1}}$)	Velocity dispersion σ_v (${\rm km\,s^{-1}}$)	Distance from centre (h^{-1} Mpc)	$N(v_{\rm p})$	Log-distance ratio η	Peculiar velocity $\langle v_{\rm p}^{\rm obj} \rangle$ (${\rm km\,s^{-1}}$)
NGC 4993	–	1	2916 ± 15	3228 ± 15	–	–	–	–	–
Abbott et al. (2017b)	–	5	–	3327 ± 72	–	–	–	–	310 ± 150
Crook et al. (2008) (LDC)	955	46	2558 ± 72	2878 ± 72	487	4.93 ± 0.53	18	0.0665 ± 0.0150	440 ± 99
Crook et al. (2008) (HDC)	763	5	3016 ± 72	3327 ± 72	160	1.13 ± 0.63	1	0.0762 ± 0.1000	582 ± 764
Lavaux & Hudson (2011)	1338	10	3026 ± 53	3338 ± 53	169	1.19 ± 0.52	2	0.0676 ± 0.0514	518 ± 394
Makarov & Karachentsev (2011)	NGC 4993	15	2935 ± 19	3248 ± 19	72	0.41 ± 0.14	1	0.0645 ± 0.0600	481 ± 448
Tully (2015)	100214	8	2997 ± 51	3310 ± 51	143	1.19 ± 0.51	3	0.1136 ± 0.0391	864 ± 297
Kourkchi & Tully (2017)	45466	22	2995 ± 32	3308 ± 32	151	0.87 ± 0.35	2	0.0676 ± 0.0514	514 ± 391
Kourkchi & Tully (2017) (Trimmed)	45466	17	2919 ± 13	3231 ± 13	52	0.43 ± 0.12	1	0.0645 ± 0.0600	479 ± 445
6dFGRS groups	GRP0056	11	3028 ± 51	3341 ± 51	166	1.10 ± 0.48	1	0.0762 ± 0.1000	585 ± 767

Downloaded from https://academic.oup.com/mnras/article-abstract/492/3/3803/5700291 by University of Queensland user on 20 April 2020

Kourkchi & Tully (2017) catalogue and using the velocity dispersion of the group as the error to account for the possibility that the group is unrelaxed (both of which are provided in Table 2). However, the fact is that even after removing possible outliers and inflating the errors, there exists a wide range of 'reasonable' observed redshifts that one could use in estimating H_0. The choices of data or outliers made when computing this adds uncertainty beyond the errors we would naively assume when inferring H_0. Given the difficulty in deciding which of the values is 'correct', this uncertainty should be folded into the analysis.

3 ESTIMATES OF THE PECULIAR VELOCITY OF THE GROUP CONTAINING NGC 4993

In this section, we turn to the arguably even less clear case of measuring the peculiar velocity (PV) of the group containing NGC 4993. The peculiar velocity of a galaxy encodes the motion induced through gravitational attraction towards dense regions of the universe in departure from the Hubble expansion. Typical line-of-sight PVs are several hundred kilometres per second, and can reach over 1000 km s^{-1} for satellite galaxies in dense regions of the universe where non-linear motions are important. Such a velocity would contribute a substantial fraction of the total velocity for a group of galaxies such as the one hosting NGC 4993, and so this absolutely must be considered when making inferences from standard sirens.

We clarify that here we are dealing with estimates of the peculiar velocity *of the group* containing NGC 4993, not of NGC 4993 itself. This is because we are using the observed redshift *of the group* which should account for/remove some of the peculiar velocity, and makes the results less susceptible to the effects of non-linear motions and large peculiar velocities. If one had an accurate measurement of the peculiar velocity of the host galaxy itself, you could use the observed redshift and peculiar velocity of the host alone to constrain H_0. Unfortunately, such an independent PV measurement does not exist for NGC 4993, and even if it did the large error would likely render it unusable. Using group properties instead allows us to average over multiple PV measurements, reducing the errors and the impact of spuriously fast-moving galaxies. It does mean however that one should take differences in group and PV catalogues into account, as we do in this work.

3.1 Peculiar velocity preliminaries

Direct measurements of the peculiar velocities of galaxies can be made using a number of different methods including the Tully–Fisher relation (Tully & Fisher 1977), Fundamental Plane (Djorgovski & Davis 1987; Dressler et al. 1987), SNe Ia (Phillips 1993), surface brightness fluctuations (Tonry & Schneider 1988), and the tip of the red giant branch (TRGB; Lee, Freedman & Madore 1993). However, those that tend to give the most accurate measurements also tend to be the hardest to obtain and least abundant. The largest single source of PVs to date is the 6-degree Field Galaxy Redshift Survey velocity sample (6dFGSv; Magoulas et al. 2012), which contains 8885 Fundamental Plane galaxies, however the typical uncertainties on the peculiar velocities in this catalogue are ~ 26 per cent and the hemispherical sky coverage leaves the measurements vulnerable to unknown systematics (Qin et al. 2018). The recently completed 2MASS Tully–Fisher survey (2MTF; Hong et al. 2019) has slightly better errors and a more homogeneous coverage, but only 2062 galaxies. The Cosmicflows-III compilation (CF3; Tully, Courtois & Sorce 2016) containing 17 669 entries, is currently the largest collection of peculiar velocity measurements. Individual measurements in here come from a variety of sources and techniques (including 6dFGSv) and so can be relatively accurate, but again the inhomogeneous selection and patchwork nature of the catalogue increases the potential for systematics.

In this work, we will use all three of these catalogues to estimate the peculiar velocity of NGC 4993. 2MTF and 6dFGSv provide measurements of the 'log-distance' ratio $\eta = \log_{10}(\mathrm{d}(z_{\rm cmb})/\mathrm{d}(\bar{z}))$; the ratio of the distance inferred from the CMB-frame redshift to the true comoving distance, where the latter is inferred from a distance indicator. This quantity is used because it is linearly related to the change in magnitude induced by a peculiar velocity (which is close to the true observed quantities for the Tully–Fisher and Fundamental Plane relationships) and is close to Gaussian distributed. The full conversion from a log-distance ratio, or any of the true observed quantities, to a PV $\langle v_{\rm p}^{\rm obj}\rangle$, results in a PDF that is closer to lognormal, with mean and maximum-likelihood values that are biased with respect to the true underlying velocity (see Scrimgeour et al. 2016 for an excellent example of this). To preserve the Gaussianity of the measurements, one could instead use the estimator of Watkins & Feldman (2015)

$$\left\langle v_{\rm p}^{\rm obj}\right\rangle = \frac{cz_{\rm mod}}{1+z_{\rm mod}}\ln(10)\eta, \tag{4}$$

where

$$z_{\rm mod} = z_{\rm cmb}\left[1+\frac{1}{2}(1-q_0)z_{\rm cmb} - \frac{1}{6}\left(1-q_0-3q_0^2+j_0\right)z_{\rm cmb}^2\right]. \tag{5}$$

For our fiducial cosmology the jerk parameter $j_0 = 1$, whilst the deceleration parameter $q_0 = \frac{1}{2}(\Omega_{\rm m} - 2\Omega_\Lambda) = -0.55$. When quoting peculiar velocities in this work, these are obtained using this estimator.

However, this estimator performs poorly under certain conditions and may introduce unwanted systematics into the estimation. This is shown in Fig. 1 where we compute the log-distance ratio, and then the Watkins & Feldman (2015) velocity, for a range of peculiar velocities and cosmological redshifts. There is a bias at low redshift arising due to the fact that the derivation of the estimator requires $v_{\rm p}^{\rm obj} \ll cz_{\rm cmb}$ and at high redshift related to the breakdown of the assumption that $v_{\rm t} = cz_{\rm obs}$ (Davis et al. 2019). For a galaxy at the observed redshift of NGC 4993 (denoted by the dotted line in Fig. 1) the bias is between 5–7 per cent and 10–15 per cent for peculiar velocities of magnitude 400 and 800 km s^{-1}, respectively. These velocities are perfectly reasonable for a galaxy such as NGC 4993 and although the bias is small compared to the typical peculiar velocity error this can be avoided entirely by working with the log-distance ratios directly, as we will demonstrate in Section 4.

Finally, CF3 presents data as distance moduli converted using a consistent cosmological model for all data sets and averaged over the individual measurements if more than one measurement is available for a given galaxy. To convert these to velocities, we first revert the distance moduli to log-distance ratios using the cosmology assumed in CF3 (flat ΛCDM with $\Omega_{\rm m} = 0.27$, $H_0 = 75$ km s^{-1} Mpc^{-1}).

3.2 Peculiar velocity estimates

In order to estimate the PV for the group containing NGC 4993 and GW170817, we need to average or interpolate over a set of nearby measurements. Abbott et al. (2017b) achieve this by placing a Gaussian weighting kernel of width $8h^{-1}$Mpc within the 6dFGSv catalogue, centred on the position of NGC 4993. From

Downloaded from https://academic.oup.com/mnras/article-abstract/492/3/3803/5700291 by University of Queensland user on 20 April 2020

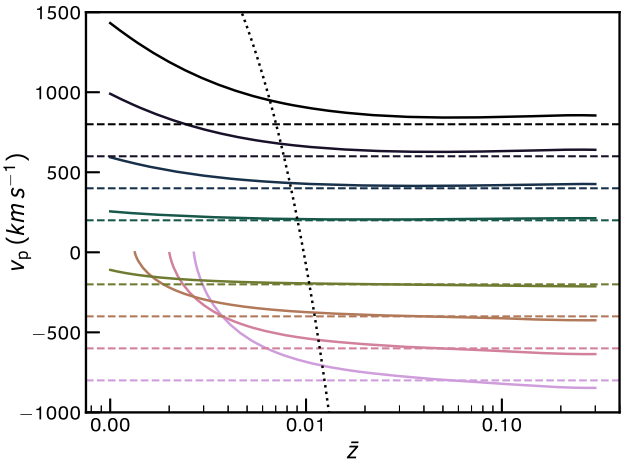

Figure 1. The performance of the Watkins & Feldman (2015) peculiar velocity estimator as a function of cosmological redshift and true peculiar velocity. The dashed lines show the input velocities, the solid lines are the estimated velocities. The dotted (almost) vertical line denotes a line of constant observed redshift (which is also a constant CMB-frame redshift), in this case that of NGC 4993, $z_{\rm obs} = 0.009727$, $z_{\rm cmb} = 0.01077$. The Watkins & Feldman (2015) estimator does not perfectly recover the true velocity given measurements of the log-distance ratio such as those from modern peculiar velocity catalogues, and is biased at low redshift when $v_{\rm p}^{\rm obj} \ll cz_{\rm cmb}$ is not satisfied, and at high redshift where it makes the implicit assumption $v_{\rm t} = cz_{\rm obs}$.

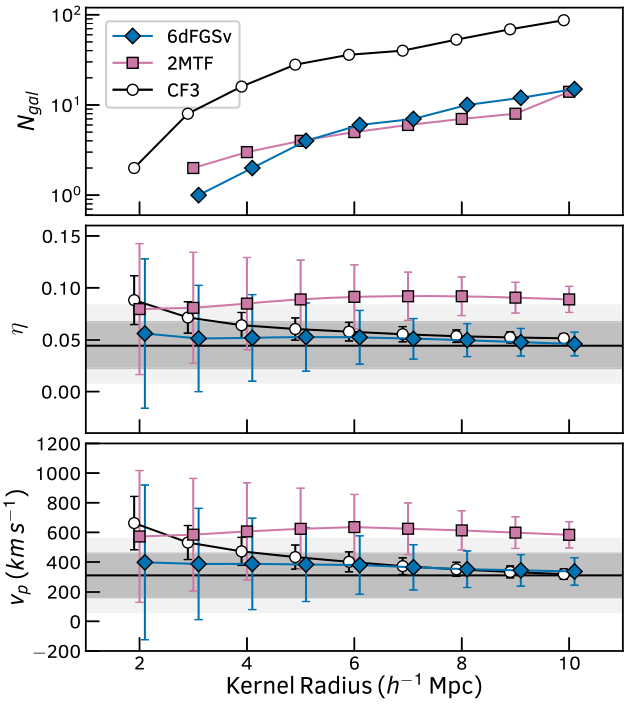

Figure 2. Peculiar velocities at the position of NGC 4993 computed using Gaussian kernels of varying radii. Different points correspond to different catalogues. The top panel shows the number of PV measurement in the catalogue within one kernel radius of NGC 4993. The middle panel shows the weighted mean and statistical uncertainty on the log-distance ratios. The bottom panel shows the weighted mean and statistical uncertainty on the PV from each catalogue calculated from the middle panel using the estimator of Watkins & Feldman (2015). The darker and lighter solid bands show the value used in Abbott et al. (2017b) with errors of 150 and 250 km s^{-1}, respectively. In the middle panel, we have propagated the velocity distribution used in Abbott et al. (2017b) to that of log-distance ratios and used the 16th, 50th, and 84th percentiles, which is necessary as the transformation in non-Gaussian.

this they quote a peculiar velocity of $\langle v_{\rm p}^{\rm obj} \rangle = 310 \pm 69\,{\rm km\,s^{-1}}$. The uncertainty $\sigma_{v_{\rm p}^{\rm obj}}$ is inflated to $150\,{\rm km\,s^{-1}}$ to account for potential systematics in their canonical model for extracting H_0, and this is increased further to $\sigma_{v_{\rm p}^{\rm obj}} = 250\,{\rm km\,s^{-1}}$ in their appendix to test the robustness of their results.

However, there are a number of choices to be made when estimating the peculiar velocity for NGC 4993. First, the Gaussian kernel used in Abbott et al. (2017b) is larger than the typical size of the groups (and the distance of NGC 4993 from the centre of those groups) identified in Section 2/Table 2 above and so a smaller scale weighting scheme might be more appropriate. Perhaps the most obvious way of ensuring consistency between the group total and peculiar velocities is instead to average only PV measurements for galaxies within the group. There is also the question of which catalogues to use in the estimation, weighing the large number of measurements in, for instance, CF3 with the clearer selection function of 2MTF. The best solution to this problem is not obvious, and as we will show below, different choices lead to substantial changes in the peculiar velocity which in turn impact the final constraints on H_0 even for the single event considered here.

We start by identifying which of the groups in Section 2 contain objects with direct PV measurements. The number of such measurements is given in Table 2 as is the average peculiar velocity. Unfortunately, the number is limited; the only group with a suitably large number is Crook et al. (2008) (LDC), however the velocities for this group may not be representative of NGC 4993 given its distance from the group centre (although this is still smaller than the smoothing scale used in Abbott et al. 2017b as mentioned above). Another promising case is that of Tully (2015), which contains three measurements in the CF3 catalogue. Although the uncertainty is quite large, we identify this combination of group observed redshift and peculiar velocity as one 'reasonable' choice.

We next turn to alternative smoothed estimates of the velocity field, using the CF3, 2MTF, and 6dFGSv catalogues. In Fig. 2, we show the log-distance ratio and peculiar velocity at the position of NGC 4993 computed using a Gaussian kernel with width varying between 2 and $10\,h^{-1}$ Mpc. On the same figure, we plot the peculiar velocity and error budget used by Abbott et al. (2017b) and the corresponding range of η values. We find differences between measurements obtained using different catalogues that are larger than the error bars on these measurements, or those adopted by Abbott et al. (2017b), would suggest.

The obvious difference in Fig. 2 is between the 2MTF and CF3/6dFGSv catalogues. We identified that this is due to a small global offset in the distances estimated from both catalogues. Qin et al. (2019) compare the 1096 common galaxies between 2MTF and CF3 (the CF3 measurements typically come from older measurements which have been updated in, and superseded by, 2MTF). They find a relationship of $\log_{10}(d_{\rm CF3}(\bar{z})) = 0.96\log_{10}(d_{\rm 2MTF}(\bar{z})) + 0.08$ where $d(\bar{z})$ is the comoving distance to the galaxy computed from the distance indicators in these catalogues. Correcting the 2MTF log-distance ratios using this equation and our fiducial cosmology, we recover PVs for NGC 4993 from 2MTF that are a much closer match to the CF3 estimate across all Gaussian kernels. This does not provide a solution to our problem however. The source of this

Downloaded from https://academic.oup.com/mnras/article-abstract/492/3/3803/5700291 by University of Queensland user on 20 April 2020

discrepancy is unclear; we would expect the 2MTF measurements for each galaxy to be more up-to-date and robust compared to those for the same object in CF3 and there are arguments for and against the zero-point calibration in both catalogues. 2MTF has a much more homogeneous distribution and selection of galaxies compared to CF3 but a smaller depth, which would both decrease and increase the relative zero-point uncertainty respectively. Again, given the difficulty in choosing which of these PV measurements is better, and the mere fact that a small calibration offset can create such a large difference, we should fold the uncertainty into our standard siren measurements.

4 CHANGES IN THE HUBBLE CONSTANT

In this section, we reproduce the analysis of Abbott et al. (2017b) with different measurements of the total and peculiar velocities for GW170817 to investigate the effects on the H_0 constraints. Our method of computing the posterior probability of H_0 given the observed gravitational-wave event and measured velocities after marginalizing over all relevant quantities is modified compared to that used in their work. The method we use here has two benefits. First, it uses the actual observed redshift $z_{\rm obs}$ and the full, correct relationship between the various redshifts given in our equation (1) rather than the approximation used in Abbott et al. (2017b) (our equation 3). Given the low redshift of NGC 4993 we expect this to have a small effect on the recovered H_0 constraints, but avoiding such approximations is preferred and does not increase the complexity of the model.

Secondly, we do not use peculiar velocities in our model and stick instead with log-distance ratios, which are much closer to the observed quantities from peculiar velocity surveys and have statistical uncertainties that are closer to being naturally Gaussian distributed. Again, this does not significantly increase the model complexity and we argue is a more natural choice for standard siren measurements. Perhaps the only caveat to this is if the estimates of the peculiar velocity come from reconstructed fields, i.e. that of Carrick et al. (2015), Graziani et al. (2019), where it is typically assumed the velocity field is Gaussian. In this case, a posterior based on the model velocity (i.e. similar to that used by Abbott et al. 2017b) may be more appropriate. See the Appendix for our version of the posterior in this scenario. It is worth noting however that such reconstructions are based either on measurements of the density field (which is non-Gaussian), or the same peculiar velocity surveys we are using directly (which also result in non-Gaussian velocities). Hence, the assumption of a Gaussian velocity field from these reconstructions could introduce systematic errors.

We start by writing the posterior probability

$$p\left(H_0|x_{\rm GW},\langle\eta\rangle,\langle z_{\rm obs}\rangle,\left\langle z_{\rm p}^{\rm Sun}\right\rangle\right)\propto p(H_0)\int\Big[p(x_{\rm GW}|d_{\rm L},\cos\iota)\times p\left(\langle\eta\rangle|H_0,d_{\rm L},z_{\rm obs},z_{\rm p}^{\rm Sun}\right)\;p(\langle z_{\rm obs}\rangle|z_{\rm obs})\,p\left(\left\langle z_{\rm p}^{\rm Sun}\right\rangle|z_{\rm p}^{\rm Sun}\right)\times p(d_{\rm L})\,p(\cos\iota)\,p(z_{\rm obs})\,p\left(z_{\rm p}^{\rm Sun}\right)\Big]\,{\rm d}d_{\rm L}\,{\rm d}\cos\iota\,{\rm d}z_{\rm obs}\,{\rm d}z_{\rm p}^{\rm Sun},\qquad(6)$$

where $d_{\rm L}$ and $\cos\iota$ are the luminosity distance and inclination of the GW event inferred from the event itself, $\langle z_{\rm obs}\rangle$, $\langle z_{\rm p}^{\rm Sun}\rangle$, and $\langle\eta\rangle$ are the measured observed redshift of the host galaxy (or the group it is in), the Sun's peculiar redshift corresponding to the CMB dipole velocity in the direction of the host (or group), and the measured log-distance ratio, respectively. $x_{\rm GW}$ are the observations of the gravitational waves made by the LIGO (LIGO Scientific Collaboration 2015) and Virgo (Acernese et al. 2015) detectors. Hence, $p(x_{\rm GW}|d,\cos\iota)$ denotes the likelihood of the observations given the distance and inclination of the merger (all other parameters related to the gravitational waveform observations, for instance the masses of the two inspiralling sources, have already been marginalized out). The uncertainty on the velocity and direction of the CMB dipole is extremely small (Planck Collaboration VI 2018) and so we treat $p(\langle z_{\rm p}^{\rm Sun}\rangle|z_{\rm p}^{\rm Sun})$ as a δ function.[2] For the remaining likelihoods, we assume Gaussian distributions, such that

$$p(\langle z_{\rm obs}\rangle|z_{\rm obs})=N[z_{\rm obs},\sigma_{z_{\rm obs}}](\langle z_{\rm obs}\rangle),\qquad(7)$$

$$p\left(\langle\eta\rangle|H_0,d_{\rm L},z_{\rm obs},z_{\rm p}^{\rm Sun}\right)=N\left[\eta\left(H_0,d_{\rm L},z_{\rm obs},z_{\rm p}^{\rm Sun}\right),\sigma_\eta\right]\times(\langle\eta\rangle)\qquad(8)$$

are the likelihoods for the observed redshift and log-distance ratio. $\sigma_{z_{\rm obs}}$ and σ_η are the measurement errors of these quantities. The final piece we need is the set of equations to compute the model log-distance ratio given the observed parameters $z_{\rm obs}$, $z_{\rm p}^{\rm Sun}$ and $d_{\rm L}$, and the parameter we want to measure, H_0. These can be derived from the definition of the log-distance ratio,

$$\eta=\log_{10}\left(\frac{{\rm d}(z_{\rm cmb})}{{\rm d}(\bar{z})}\right)=\log_{10}\left((1+z_{\rm obs})\frac{{\rm d}(z_{\rm cmb})}{d_{\rm L}}\right),\qquad(9)$$

where

$${\rm d}(z_{\rm cmb})=\frac{c}{H_0}\int_0^{\frac{1+z_{\rm obs}}{1+z_{\rm p}^{\rm Sun}}-1}\frac{{\rm d}z}{E(z)},\qquad(10)$$

and $E(z)=\sqrt{\sum_i\Omega_i(1+z)^{-3(1+w_i)}}$ is the usual redshift-dependent part of the expansion rate. Herein, we assume a flat ΛCDM cosmological model, although this could easily be expanded to incorporate alternative cosmological models. The above framework can also be modified to work for model peculiar velocities rather than log-distance ratios, but without the need to make any of the approximations used in Abbott et al. (2017b). This is shown in the Appendix.

Although the above method may seem more complex than that used in Abbott et al. (2017b), in practice it does not take much longer to compute (the redshift–distance relationship can be spline interpolated for fast inversion for any value of H_0). Crucially however, it makes no assumptions about the relationship between the redshifts and velocities of interest, which may otherwise introduce systematic errors, and it works more closely with the observed quantities of the host, namely the group observed redshift and the log-distance ratio. We investigate how our modified posterior compares to that of Abbott et al. (2017b) below. We found no dependence of the results in this work on the assumed value of $\Omega_{\rm m}$, as would be expected given the low redshift of NGC 4993.[3]

Rather than repeat the full analysis of the gravitational-wave event to evaluate $p(x_{\rm GW}|d_{\rm L},\cos\iota)$ and $p(H_0|x_{\rm GW},\langle z_{\rm obs}\rangle,\langle z_{\rm p}^{\rm Sun}\rangle,\langle\eta\rangle)$, we

[2]We have included it in our posterior calculation as it should be included in the case where the host galaxy is not known. Additionally, we have not considered uncertainty in the angular position of the host group. If we did there would be some uncertainty on $z_{\rm p}^{\rm Sun}$ even if the direction and velocity of the CMB dipole were perfectly known.

[3]For future standard sirens at higher redshift where this effect may not be negligible, one could follow the method used in the cosmological analysis of SNe Ia and reduce the cosmological dependence of the fit for the Hubble constant without resorting to the approximation ${\rm d}(z_{\rm cmb})\approx\frac{cz_{\rm cmb}}{H_0}$ by instead using ${\rm d}(z_{\rm cmb})\approx\frac{cz_{\rm mod}}{H_0}$ with $z_{\rm mod}$ given by equation (5).

Downloaded from https://academic.oup.com/mnras/article-abstract/492/3/3803/5700291 by University of Queensland user on 20 April 2020

will make use of the posterior samples for GW170817 provided by both the LIGO collaboration[4] and from Hotokezaka et al. (2019). The latter includes additional information on the source inclination that significantly strengthens the constraints on H_0. In using these samples to evaluate equation (6), we perform an MCMC[5] over the parameters $z_{\rm obs}$ and H_0 and at each likelihood evaluation we draw from the marginalized posterior samples for $d_{\rm L}$ and $\cos\iota$. The combined posterior from this procedure then approximates the full posterior for all four parameters as if we had fit the GW signal directly.

The accuracy of this approximation depends on how well the finite number of posterior samples for $d_{\rm L}$ and $\cos\iota$ represents the true posterior, which we test by repeating the canonical analyses of Abbott et al. (2017b) and Hotokezaka et al. (2019) (which uses the approximate equation 3). Doing so, setting $cz_{\rm cmb} = 3327 \pm 72\,{\rm km\,s^{-1}}$ and $\langle v_{\rm p}^{\rm obj}\rangle = 310 \pm 150\,{\rm km\,s^{-1}}$, we find $H_0 = 69.8^{+11.0}_{-7.2}\,{\rm km\,s^{-1}\,Mpc^{-1}}$ and $H_0 = 68.3^{+4.5}_{-4.4}\,{\rm km\,s^{-1}\,Mpc^{-1}}$, respectively. Our errors are slightly smaller than those found in Abbott et al. (2017b) ($H_0 = 70.0^{+12.0}_{-8.0}\,{\rm km\,s^{-1}\,Mpc^{-1}}$) but fully consistent with Hotokezaka et al. (2019) ($H_0 = 68.1^{+4.5}_{-4.3}\,{\rm km\,s^{-1}\,Mpc^{-1}}$). We attribute the differences to the finite number of samples in the GW posterior chains. Our estimate of the distance to GW170817 from Abbott et al. (2017b) is $d_{\rm L} = 44.2^{+2.3}_{-6.5}\,{\rm Mpc}$ (to be compared to the quoted value of $d_{\rm L} = 43.8^{+2.9}_{-6.9}\,{\rm Mpc}$); the small shift in the peak and slight underestimation of the errors is likely because the posterior samples do not fully represent the long tail of the true luminosity distance distribution. This in turn leads to small differences in the recovered H_0 posterior. For fairness, we compare all our results for different cases below to *our* results for the canonical model, rather than the quoted results.

4.1 Comparing Bayesian models

We begin by comparing the results using our preferred Bayesian model presented above to that used in Abbott et al. (2017b) and Hotokezaka et al. (2019). In this fit (and all fits from here on), we use a prior $p(H_0) \propto 1/H_0$, a volumetric prior $p(d_{\rm L}) \propto d_{\rm L}^2$ and a flat prior $p(z_{\rm obs})$ with $cz_{\rm obs} \in [2000, 4000]\,{\rm km\,s^{-1}}$. For comparison, we start with $\langle cz_{\rm obs}\rangle = 3016 \pm 72$ and $\langle\eta\rangle = 0.049 \pm 0.023$, which are the values derived using exactly the same group and peculiar velocity catalogue as Abbott et al. (2017b) and where we have adopted an error on the log-distance ratio that is close to that used for the velocity in Abbott et al. (2017b) [applying the Watkins & Feldman (2015) estimator to this value for the error returns $154\,{\rm km\,s^{-1}}$].

Using the above procedure and our fiducial cosmology, we find $H_0 = 67.9^{+4.6}_{-4.5}\,{\rm km\,s^{-1}\,Mpc^{-1}}$ and $H_0 = 69.5^{+11.7}_{-7.3}\,{\rm km\,s^{-1}\,Mpc^{-1}}$ with and without the extra constraints on the source inclination, respectively. There is a small decrease in the maximum a posteriori values of $< 0.5\,{\rm km\,s^{-1}\,Mpc^{-1}}$ compared to the canonical model, which is not significant compared to the uncertainties and the 68 per cent equal likelihood bounds cover a nearly identical range of H_0 values. However, we emphasize again that our model makes fewer assumptions and is closer to the observed quantities and so will be preferable as more gravitational waves are detected, constraints on the Hubble constant become tighter and the impact of potential systematic errors becomes more important.

[4]These can be found at https://dcc.ligo.org/LIGO-P1800061/public/. We use the samples assuming a 'high-spin' prior.

[5]We use the publicly available EMCEE PYTHON routine (Foreman-Mackey et al. 2013).

4.2 Different choices of recession and peculiar velocity

We next look at the results of using alternative estimates of the total and peculiar velocities of NGC 4993 when constraining H_0. We test a wide range of cases based on the results of Sections 2 and 3, first using the observed redshift and mean log-distance ratio for seven of the groups listed in Table 2 [all but Crook et al. 2008 (LDC), which as explained in Section 2 has a redshift far from that of NGC 4993], and then combining these different group observed redshifts with the log-distance ratios calculated from the three peculiar velocity catalogues in Section 3 with Gaussian Kernels of different widths. We ultimately obtained posterior distributions for the Hubble constant for all possible combinations of group catalogue, peculiar velocity survey and Gaussian Kernel with width between 2 and $8\,h^{-1}\,{\rm Mpc}$, which combined with the constraints using only the group catalogues gives a total of 154 different scenarios. In all cases we place a minimum possible error on the observed redshift (times the speed of light) of $50\,{\rm km\,s^{-1}}$ and on the log-distance ratio of 0.023, similar to what was done in Abbott et al. (2017b) and mimicking one potential way that we might try (unsuccessfully, as we will show) to mitigate potential systematics.

Descriptions of five of the additional cases, any of which we argue could equally be chosen when analysing event GW170817, are presented in Table 3 along with the resulting H_0 constraints with and without the extra information on the source inclination from Hotokezaka et al. (2019). In Fig. 3, we show the marginalized posteriors on H_0 and the model log-distance ratio of NGC 4993 for these cases. We note that the value of η given in these figures are those computed for each of the posterior samples using equation (9). By definition the distribution of these should match the assumed probability distribution of the observed log-distance ratio. We include these in Fig. 3 to highlight the strong dependence of the Hubble constant on the choice of observations.

From the results presented in this figure, we see that different choices or determinations of the total and peculiar velocities of NGC 4993 result in different constraints that, while consistent at the 68 per cent confidence level (although only just for the more constrained data from Hotokezaka et al. 2019), have a spread larger than the error from the Canonical analysis (Case 1) would suggest. It is also interesting to note that of the possible cases presented here (and compared to the majority of the alternative cases we tested) the canonical analysis produces the largest H_0 constraints. This is a result of the relatively large observed redshift and small log-distance ratio (peculiar velocity) used in this analysis.

It is clear that in order for robust constraints to be obtained we need to better understand which of the techniques for calculating the group observed redshift and log-distance ratio or peculiar velocity gives the most reliable and accurate results, or better account for our uncertainty on these quantities. This is more complicated than simply increasing the standard deviation on our measurement of the peculiar velocity. For the case of GW170817 alone this is demonstrated by the fact that we have included conservative lower limits on the errors for all our different combinations and that Abbott et al. (2017b) inflated the peculiar velocity errors even further to test the robustness of their constraints, but these results still do not encompass the spread seen in Fig. 3. In the following section, we instead suggest the use of Bayesian model averaging (see Parkinson & Liddle 2013 for a review) to combine all the cases we test here into a more representative constraint on H_0.

Downloaded from https://academic.oup.com/mnras/article-abstract/492/3/3803/5700291 by University of Queensland user on 20 April 2020

Table 3. Constraints on H_0 from GW170817 and NGC 4993 assuming different combinations of observed redshift and log-distance ratio. Where only a group reference is provided as a description, this indicates use of the group observed redshift and mean CF3 log-distance ratio from Table 2. Where a group reference and a PV catalogue are provided, this indicates the use of the group observed redshift and log-distance ratio from the catalogue using a Gaussian kernel of radius R. For each case, we provide the values and errors used in constraining H_0. The last two columns give the maximum a posteriori value and 68 per cent equal likelihood bounds on H_0 without and with additional constraints on the source inclination angle, respectively [and so the left and right sub-columns correspond to the analyses of Abbott et al. (2017b) and Hotokezaka et al. (2019), respectively]. The first row is where we use the same group and peculiar velocity catalogues/methods used in these previous works, but with our updated Bayesian model.

Case no.	Description	Observed redshift $\langle z_{\rm obs}\rangle$ ($\times 10^{-5}$)	Log-distance ratio $\langle\eta\rangle$	Hubble constant H_0 (km s^{-1} Mpc^{-1})	
				GW	GW + VLBI
1.	Canonical: Crook et al. (2008) (HDC) + 6dFGSv ($R = 8\,h^{-1}$ Mpc)	1006 ± 24	0.049 ± 0.023	$69.5^{+11.7}_{-7.3}$	$67.9^{+4.6}_{-4.5}$
2.	Tully (2015)	1000 ± 17	0.114 ± 0.039	$60.1^{+11.3}_{-7.7}$	$58.0^{+6.1}_{-5.3}$
3.	Kourkchi & Tully (2017)	999 ± 11	0.068 ± 0.051	$67.2^{+14.1}_{-10.1}$	$64.6^{+8.7}_{-7.5}$
4.	6dFGRS + CF3 ($R = 2\,h^{-1}$ Mpc)	1010 ± 17	0.089 ± 0.024	$63.5^{+10.6}_{-6.5}$	$62.3^{+4.1}_{-4.1}$
5.	Kourkchi & Tully (2017) (Trimmed) + 6dFGSv ($R = 8\,h^{-1}$ Mpc)	974 ± 17	0.049 ± 0.023	$67.4^{+11.0}_{-7.1}$	$65.9^{+4.3}_{-4.3}$
6.	Crook et al. (2008) (HDC) + 2MTF ($R = 8\,h^{-1}$ Mpc)	1006 ± 24	0.091 ± 0.023	$63.2^{+10.2}_{-6.7}$	$61.7^{+4.1}_{-4.1}$

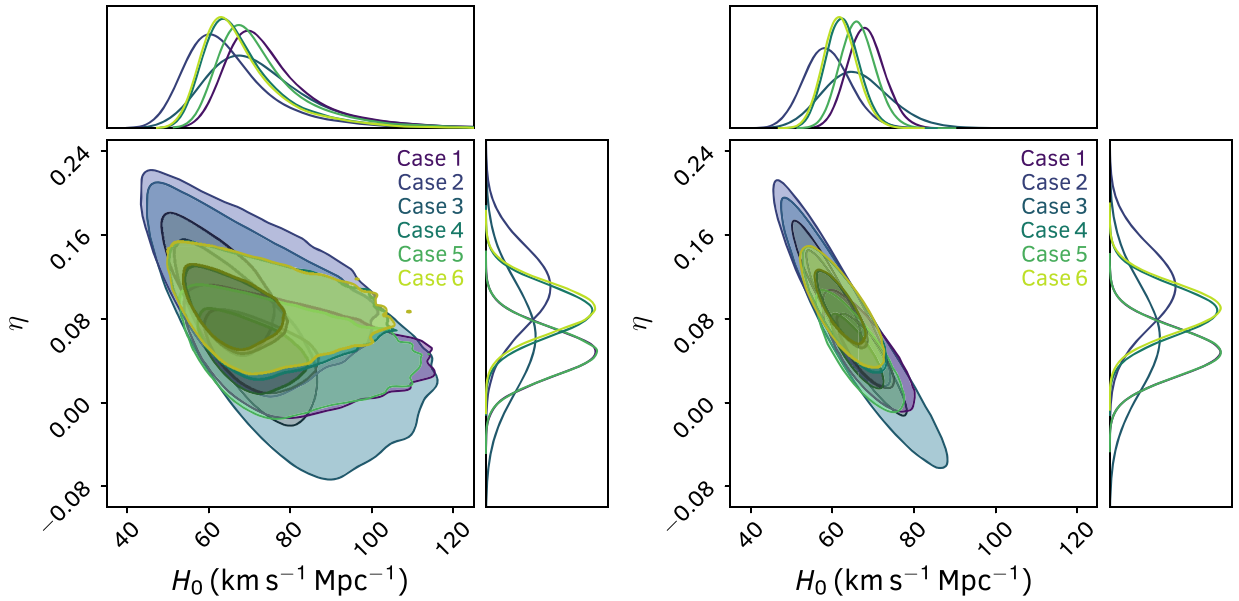

Figure 3. Marginalized constraints on the Hubble constant H_0, and corresponding model log-distance ratios η, of NGC 4993 from the standard siren measurement of GW170817 for the six different cases listed in Table 3. The left plot shows the constraints without any additional information on the viewing angle (Abbott et al. 2017b), whilst right shows the tighter constraints when this information is included (Hotokezaka et. al. 2019).

4.3 Bayesian model averaged Hubble constant

One way to evaluate the relative weight we should give to each H_0 posterior when dealing with uncertainty in the true observed redshift or log-distance ratio of the source is the Bayesian evidence. For a given model $\mathcal{M}_i$, this is the probability of the model given our data $p(\mathcal{M}_i|D)$. In our scenario, we have 154 different models corresponding to our seven different group catalogues, three peculiar velocity surveys, and seven kernel radii. Bayesian model averaging uses the evidence as a way to perform a weighted average over all the models and create a unified posterior $p(\theta|D)$ that accounts for our uncertainty regarding which model is correct. Mathematically, we write this in terms of the parameter posteriors $p(\theta|D, \mathcal{M}_i)$ for each model and the evidence,

$$p(\theta|D) = \frac{\sum_i p(\theta|D, \mathcal{M}_i)p(\mathcal{M}_i|D)}{\sum_i p(\mathcal{M}_i|D)}. \quad (11)$$

We first compute the evidence for each of the cases.[6] We then produce a combined posterior by weighting the samples from each individual model by the evidence. The result of this procedure is

[6]We do this using the implementation of Single Ellipsoid Nested Sampling (Mukherjee, Parkinson & Liddle 2006) in the PYTHON package NESTLE found here: http://kylebarbary.com/nestle/. The way nested sampling works means we can no longer sample from the posterior chains for GW170817 to obtain $\cos\iota$ and $d_{\rm L}$ inside the likelihood evaluation. Instead, we use Gaussian kernel density estimation (KDE) to reproduce the 2D likelihood surface of these two parameters and perform the nested sampling over these, H_0 and $z_{\rm obs}$ (so four dimensions in total), evaluating the likelihood using the KDE for $\cos\iota$ and $d_{\rm L}$ at every point. This produces results consistent with the sampling method used previously. Future studies could incorporate the evidence calculation directly when fitting the GW data, but the approximate method here is suitable for the illustrative purposes of this work.

Downloaded from https://academic.oup.com/mnras/article-abstract/492/3/3803/5700291 by University of Queensland user on 20 April 2020

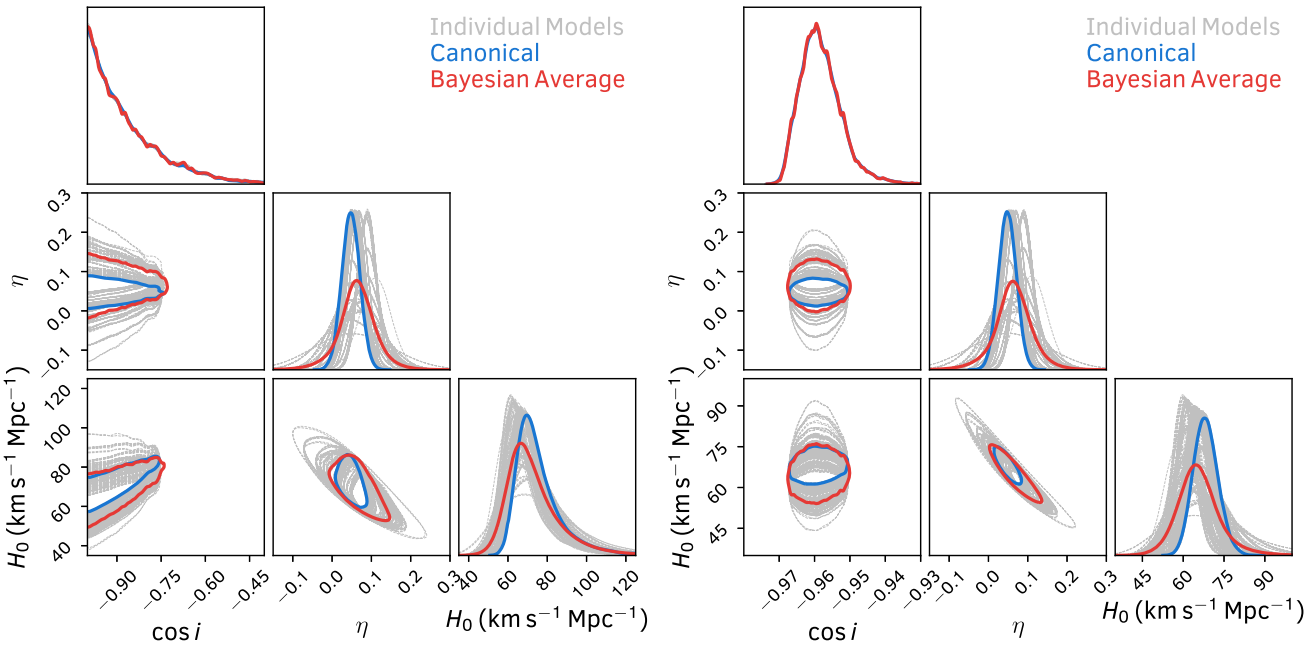

Figure 4. Constraints on the Hubble constant H_0 and GW source inclination $\cos\iota$, and the corresponding model log-distance ratio of NGC 4993 η using Bayesian model averaging to encapsulate our uncertainty on the different measurements of the total observed velocity and log-distance ratio. The left plot shows the constraints without any additional information on the viewing angle (i.e. corresponding to Abbott et al. 2017b), whilst right shows the tighter constraints when this information is included (Hotokezaka et al. 2019). In both cases, the canonical model from these references is shown in blue, the various individual models from this work (using different combination of observed redshift and log-distance ratio) are in grey. The Bayesian Average of the individual models is shown in red. Performing a weighted average of the different models more accurately accounts for our uncertainty in the observed quantities, giving more robust constraints.

shown in Fig. 4. The combined posterior more fully represents our true uncertainty on the Hubble constant. We obtain averaged marginalized constraints of $H_0 = 66.8^{+13.4}_{-9.2}\,\mathrm{km\,s^{-1}\,Mpc^{-1}}$; and $H_0 = 64.8^{+7.3}_{-7.2}\,\mathrm{km\,s^{-1}\,Mpc^{-1}}$ when additional information on the viewing angle is included. Whilst these are consistent with the canonical results of Abbott et al. (2017b) and Hotokezaka et al. (2019), accounting for our uncertainty in the total observed and peculiar velocities of NGC 4993 has decreased the maximum a posteriori value in both cases by $\sim 3\,\mathrm{km\,s^{-1}\,Mpc^{-1}}$ because the majority of models have lower observed redshifts and larger log-distance ratios than the canonical model.

Averaging over our model uncertainty has also increased the width of the 68 per cent confidence interval by ~ 35 per cent and ~ 68 per cent without and with the extra information on the source inclination, respectively. In the latter case, with the source inclination known much more precisely, the unknown peculiar velocity of NGC 4993 is the dominant source of uncertainty and has the potential to strongly bias our results. Performing an average over all the various measurements should mitigate against this quite well, but substantially increases the uncertainty on the Hubble constant. This demonstrates that the accuracy with which we can measure and model the velocity field in the local Universe will remain an important consideration in the error budget for future standard siren measurements and is an area where improvement could be made. From Fig. 4, it is also apparent that simply increasing the uncertainty on the log-distance ratio or peculiar velocity, as tested in Abbott et al. (2017b), is not the optimal way to account for this; the distribution of model log-distance ratios after Bayesian Averaging is non-Gaussian and has significant density in the tails of the distribution that would not be captured by placing a lower limit on the uncertainty of the log-distance ratio or peculiar velocity in either our model (equation 8) or that of Abbott et al. (2017b).

Finally, Fig. 5 shows a comparison of our new results for the Hubble constant from GW170817 with and without the inclusion of additional VLBI observations and modelling of the radio afterglow against those from the Planck Collaboration VI (2018) and the SH0ES collaboration (Riess et al. 2019). The maximum a posteriori value of H_0 is in better agreement with the Planck Collaboration VI (2018) than Riess et al. (2019), particularly now that our Bayesian Average has lowered this compared to the canonical constraints. However, our results also still agree with the SH0ES at just over 1σ even for the more constrained case based on the analysis of Hotokezaka et al. (2019). This would not be the case if we had not marginalized over our uncertainty in the observed properties of NGC 4993; there are a number of choices of observed redshift and peculiar velocity that, if treated the same way as the canonical model, would have led to a larger discrepancy between the constraints from GW170817 and SH0ES. For example, cases 2, 4, and 6 in Table 3 would all be discrepant with SH0ES by $>2\sigma$ if treated in isolation. More completely including and accounting for uncertainty in the observed quantities is of key importance for nearby standard siren measurements to ensure we do not reach biased conclusions. One silver lining is that as more local measurements are obtained, the random component of the peculiar velocity errors will average out, however this will require a considerable number of independent measurements and they will still remain susceptible to coherent systematic errors. Standard sirens at larger distances will also be less affected by changes in the peculiar velocity correction.

Downloaded from https://academic.oup.com/mnras/article-abstract/492/3/3803/5700291 by University of Queensland user on 20 April 2020

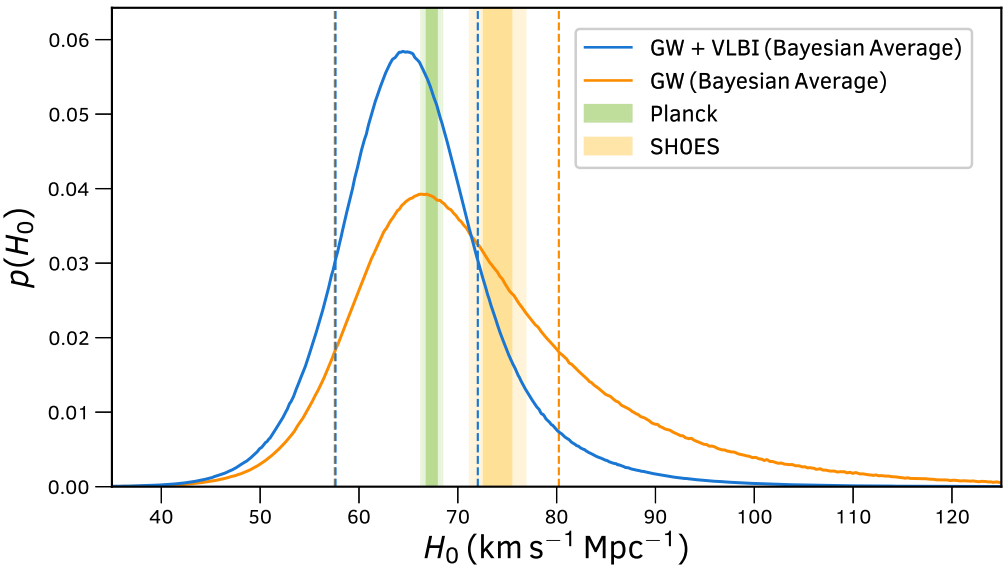

Figure 5. Posterior probability distribution functions for the Hubble constant from our re-analysis of GW170817 and the properties of its host NGC 4993. The blue and orange curves show the constraints with and without the inclusion of extra information on the source inclination from observations of the radio afterglow, respectively, the vertical dashed lines show the upper and lower equal likelihood bounds encapsulating 68 per cent of the posteriors. For both cases, we have performed a Bayesian Average over the 154 different combinations of total observed redshift and log-distance ratio identified in this work. The vertical bars show the 1 and 2σ bounds on the Hubble constant from the Planck Collaboration VI (2018) (green) and the local distance ladder as measurement by the SH0ES collaboration (orange; Riess et al. 2019).

4.3.1 Comparison to other recent results

Concurrent to this work, two other studies were produced that examined how different choices for the peculiar velocity of NGC 4993 used to analyse GW170817 affected the Hubble Constant constraints. Whereas we have focused on direct estimates of galaxy peculiar velocities from secondary distance indicators, Mukherjee et al. (2019) look at reconstruction of the local velocity field, using a new algorithm that forward models the observed redshift distribution of galaxies using *N*-body methods, which simultaneously recovers the real-space overdensity and velocity fields. Applying a newly derived velocity correction to the data from Hotokezaka et al. (2019) they arrive at $H_0 = 69.3^{+4.5}_{-4.0}$ km s^{-1} Mpc^{-1} to be compared to our result of $H_0 = 64.8^{+7.3}_{-7.2}$ km s^{-1} Mpc^{-1}. The two results are consistent at the 1σ level, with our results reporting larger error bars and a lower value of H_0. This is not surprising given that the peculiar velocity at the location of NGC 4993 reported in Mukherjee et al. (2019) is very similar to that used in the canonical analysis, whereas we find that the majority of alternative data choices give a larger peculiar velocity and hence smaller H_0. However, our method of averaging over many choices of peculiar velocity data ensures consistency between the constraints. The benefit of using the reconstructed field is that it provides a consistent and coherent interpolation of the velocity field across a wide cosmological volume where the selection functions inherent in the data can be modelled and included. An interesting avenue for future work would be to see how the reconstructed velocity field changes when the choice of data to fit against is changed (in a similar vein to what we have investigated here), and whether there are differences that arise in the recovered peculiar velocity that need to be accounted for.

The second study, Nicolaou et al. (2019) has a more sizeable overlap with our work. They investigate how the H_0 constraints change when the smoothing scale used to infer the peculiar velocity from the 6dFGSv peculiar velocity catalogue is included as a free parameter in the Bayesian model. They obtain $H_0 = 68.6^{+14.0}_{-8.5}$ km s^{-1} Mpc^{-1} using the original Abbott et al. (2017b) data, compared to our new result of $H_0 = 66.8^{+13.4}_{-9.2}$ km s^{-1} Mpc^{-1}. Again the two results are consistent, with our study finding a slightly lower value. Both studies have accounted for variations in the smoothing scale on the recovered values of H_0, with Nicolaou et al. (2019) adopting a more rigourous marginalization over this choice compared to our Bayesian average (which could be likened more to a grid based marginalization). However, in our study we also account for changes in the input peculiar velocity catalogue in addition to the smoothing scale applied to the catalogue; as both 2MTF and CF3 (for small smoothing lengths) prefer larger peculiar velocities than 6dFGSv, we find a lower value for H_0. An obvious way forward for future work would be to combine both our methodologies and adopt the smoothing scale as a free parameter in the Bayesian model for each choice of peculiar velocity catalogue *and* then average over the choice of input data. This would significantly reduce the number of unique MCMC chains/evidence calculations used in our work, reducing the computational cost.

5 CONCLUSIONS

Standard siren measurements of the Hubble constant have the potential to rival those from standard candles or rulers. However, current measurements are limited by our knowledge of the host velocities, in particular the peculiar velocity. In this work, we have demonstrated that current measurements of the observed redshift and peculiar velocity (or rather log-distance ratio) obtained using different methods and data for the single standard siren measurement from GW170817 and NGC 4993 contain considerable uncertainty that is not, and likely cannot, be fully understood. This leads to uncertainties on the recovered Hubble constant larger than we would naively assume.

Downloaded from https://academic.oup.com/mnras/article-abstract/492/3/3803/5700291 by University of Queensland user on 20 April 2020

We have presented one way to account for this uncertainty using Bayesian model averaging and obtain constraints of $H_0 = 66.8^{+13.4}_{-9.2}\,\mathrm{km\,s^{-1}\,Mpc^{-1}}$ and $H_0 = 64.8^{+7.3}_{-7.2}\,\mathrm{km\,s^{-1}\,Mpc^{-1}}$ without and with the inclusion of high-resolution measurements of the radio counterpart. These are lower and have substantially larger errors than those originally quoted in Abbott et al. (2017b) and Hotokezaka et al. (2019). In the course of this work, we have also developed a model for the posterior distribution of the Hubble constant that works more closely with the observed quantities from galaxy redshift and peculiar velocity surveys. However, the main conclusion from this work is that greater understanding is needed of the limitations of current methods to obtain total and peculiar velocities for standard siren measurements, how these compare, and how these can be combined. This will remain an important consideration in the future as more standard sirens are detected, at least until we have a large enough number of measurements, or more measurements at larger observed redshifts, to mitigate the effects of peculiar velocity errors.

ACKNOWLEDGEMENTS

We thank David Parkinson for useful discussions. We are also especially grateful to Kenta Hotokezaka and the LIGO Collaboration for providing their posterior samples for GW170817 and to Alex Merson, D. Heath Jones, Matthew Colless, and the authors of all the publicly available group and peculiar velocity catalogues used in this work. This research would not have been possible without these data.

This research was supported by the Australian Government through the Australian Research Council's Laureate Fellowship funding scheme (project FL180100168). This research has made use of NASA's Astrophysics Data System Bibliographic Services and the `astro-ph` pre-print archive at https://arxiv.org/. Plots in this paper were made using the MATPLOTLIB plotting library (Hunter 2007) and the CHAINCONSUMER package (Hinton 2016).

REFERENCES

Abbott B. P. et al., 2017a, Phys. Rev. Lett., 119, 161101
Abbott B. P. et al., 2017b, Nature, 551, 85
Abbott B. P. et al., 2017c, ApJ, 848, L12
Abbott B. P. et al., 2019, Phys. Rev. X, 9, 11001
Acernese F. et al., 2015, Class. Quantum Gravity, 32, 24001
Cantiello M. et al., 2018, ApJ, 854, L31
Carrick J., Turnbull S. J., Lavaux G., Hudson M. J., 2015, MNRAS, 450, 317
Chen H.-Y., Fishbach M., Holz D. E., 2018, Nature, 562, 545
Crook A. C., Huchra J. P., Martimbeau N., Masters K. L., Jarrett T., Macri L. M., 2007, ApJ, 655, 790
Crook A. C., Huchra J. P., Martimbeau N., Masters K. L., Jarrett T., Macri L. M., 2008, ApJ, 685, 1320
Davis T. M., Lineweaver C. H., 2004, Publ. Astron. Soc. Aust., 21, 97
Davis T. M., Hinton S. R., Howlett C., Calcino J., 2019, MNRAS, 490, 2948
Djorgovski S., Davis M., 1987, ApJ, 313, 59
Dressler A., Lynden-Bell D., Burstein D., Davies R. L., Faber S. M., Terlevich R., Wegner G, 1987, ApJ, 313, 42
Fishbach M. et al., 2019, ApJ, 871, L13
Foreman-Mackey D., Hogg D. W., Lang D. et al., 2013, PASP, 125, 306
Freedman W. L. et al., 2019, ApJ, 882, 34
Graziani R. et al., 2019, MNRAS, 488
Hinton S. R., 2016, J. Open Source Softw., 1, 00045
Hjorth J. et al., 2017, ApJ, 848, L31
Hong T. et al., 2019, MNRAS, 487
Hotokezaka K. et al., 2019, Nat. Astron., 3
Huchra J. P. et al., 2012, ApJS, 199, 26
Hunter J. D., 2007, Comput. Sci. Eng., 9, 90
Im M. et al., 2017, ApJ, 849, L16
Jones D. H. et al., 2009, MNRAS, 399, 683
Kourkchi E., Tully R. B., 2017, ApJ, 843, 16
Lavaux G., Hudson M. J., 2011, MNRAS, 416, 2840
Lee M. G., Freedman W. L., Madore B. F., 1993, ApJ, 417, 553
LIGO Scientific Collaboration, 2015, Class. Quantum Gravity, 32, 74001
Magoulas C. et al., 2012, MNRAS, 427, 245
Makarov D., Karachentsev I., 2011, MNRAS, 412, 2498
Mortlock D. J., Feeney S. M., Peiris H. V., Williamson A. R., Nissanke S. M., 2019, Phys. Rev. D, 100, 103523
Mukherjee P., Parkinson D., Liddle A. R., 2006, ApJ, 638, L51
Mukherjee S., Lavaux G., Bouchet F. R., Jasche J., Wandelt B. D., Nissanke S. M., Leclercq F., Hotokezaka K., 2019, preprint (arXiv:1909.08627)
Nicolaou C., Lahav O., Lemos P., Hartley W., Braden J., 2019, preprint (arXiv:1909.09609)
Parkinson D., Liddle A. R., 2013, Stat. Anal. Data Min.: ASA Data Sci. J., 9, 3
Phillips M. M., 1993, ApJ, 413, L105
Planck Collaboration VI, 2018, preprint (arXiv:1807.06209)
Qin F., Howlett C., Staveley-Smith L., Hong T., 2018, MNRAS, 477, 5150
Qin F., Howlett C., Staveley-Smith L., Hong T., 2019, MNRAS, 482, 1920
Riess A. G., Casertano S., Yuan W., Macri L. M., Scolnic D., 2019, ApJ, 876, 85
Sandage A., Tammann G. A., 1990, ApJ, 365, 1
Scrimgeour M. I. et al., 2016, MNRAS, 455, 386
Shafieloo A., Keeley R. E., Linder E. V., 2018, preprint (arXiv:1812.07775)
Soares-Santos M. et al., 2019, ApJ, 876, L7
Tonry J., Schneider D. P., 1988, AJ, 96, 807
Tonry J. L., Blakeslee J. P., Ajhar E. A., Dressler A., 2000, ApJ, 530, 625
Tully R. B., 2015, AJ, 149, 171
Tully R. B., Fisher J. R., 1977, A&A, 500, 105
Tully R. B., Shaya E. J., Karachentsev I. D., Courtois H. M., Kocevski D. D., Rizzi L., Peel A., 2008, ApJ, 676, 184
Tully R. B., Courtois H. M., Sorce J. G., 2016, AJ, 152, 50
Watkins R., Feldman H. A., 2015, MNRAS, 450, 1868
York D. G. et al., 2000, AJ, 120, 1579
Zhang X.-N., Wang L.-F., Zhang J.-F., Zhang X., 2019, Phys. Rev. D, 99, 63510

APPENDIX A: BAYESIAN MODEL FOR H_0 USING PECULIAR VELOCITY INSTEAD OF LOG-DISTANCE RATIO

In this appendix, we present the posterior probability of H_0 based on the framework in Section 4 given measurements of the object's peculiar velocity as opposed to the log-distance ratio. This may be appropriate for the case where the peculiar velocity of the group containing the host galaxy or object is obtained from reconstructions of the velocity field as opposed to direct measurements from peculiar velocity surveys such as CF3, 2MTF, or 6dFGSv. The method is very similar to that originally used in Abbott et al. (2017b), however we treat the object's peculiar velocity as the measurement to fit against, rather than the observed redshift, and we make no approximations on the relationship between the various redshifts and velocities.

We start by writing the posterior probability

$$p\left(H_0|x_{\rm GW}, \left\langle v_{\rm p}^{\rm obj}\right\rangle, \langle z_{\rm obs}\rangle, \left\langle z_{\rm p}^{\rm Sun}\right\rangle\right) \propto p(H_0)\int\Big[p(x_{\rm GW}|d_{\rm L},\cos\iota) \times p\left(\left\langle v_{\rm p}^{\rm obj}\right\rangle|H_0,d_{\rm L},z_{\rm obs},z_{\rm p}^{\rm Sun}\right)\, p(\langle z_{\rm obs}\rangle|z_{\rm obs})\, p\left(\left\langle z_{\rm p}^{\rm Sun}\right\rangle|z_{\rm p}^{\rm Sun}\right) \times p(d_{\rm L})p(\cos\iota)p(z_{\rm obs})p\left(z_{\rm p}^{\rm Sun}\right)\Big]\,{\rm d}d_{\rm L}\,{\rm d}\cos\iota\,{\rm d}z_{\rm obs}\,{\rm d}z_{\rm p}^{\rm Sun}, \quad \text{(A1)}$$

Downloaded from https://academic.oup.com/mnras/article-abstract/492/3/3803/5700291 by University of Queensland user on 20 April 2020

where $\langle v_{\rm p}^{\rm obj} \rangle$ is the measured peculiar velocity of the object and other terms are as defined in Section 4. If we adopt a Gaussian distribution for the object's measured peculiar velocity,

$$p\left(\left\langle v_{\rm p}^{\rm obj}\right\rangle | H_0, d_{\rm L}, z_{\rm obs}, z_{\rm p}^{\rm Sun}\right) = N\left[v_{\rm p}^{\rm obj}\left(H_0, d_{\rm L}, z_{\rm obs}, z_{\rm p}^{\rm Sun}\right), \sigma_{v_{\rm p}^{\rm obj}}\right] \times \left(\left\langle v_{\rm p}^{\rm obj}\right\rangle\right), \tag{A2}$$

where $\sigma_{v_{\rm p}^{\rm obj}}$ is the measurement error on the object's peculiar velocity, all that remains is for us to write the model peculiar velocity in terms of the parameters H_0, $d_{\rm L}$, $z_{\rm obs}$, and $z_{\rm p}^{\rm Sun}$. We do this by first computing the object's peculiar redshift

$$z_{\rm p}^{\rm obj} = \frac{1 + z_{\rm obs}}{(1 + \bar{z}(d_{\rm L}, H_0, z_{\rm obs}))\left(1 + z_{\rm p}^{\rm Sun}\right)} - 1, \tag{A3}$$

where the cosmological redshift $\bar{z}(d_{\rm L}, H_0, z_{\rm obs})$ is computed by numerically inverting the redshift–distance relation. The object's peculiar redshift is then converted to a peculiar velocity using

$$v_{\rm p}^{\rm obj} = c\frac{\left(1 + z_{\rm p}^{\rm obj}\right)^2 - 1}{\left(1 + z_{\rm p}^{\rm obj}\right)^2 + 1}. \tag{A4}$$

Although this seem more complex than the model used in Abbott et al. (2017b), it is not computationally demanding or difficult to implement; the numerical inversion of the redshift–distance relationship can be achieved extremely efficiently using, for instance, spline interpolation. However, this model makes no assumptions about the relationship between the various redshifts which could bias constraints from standard sirens.

This paper has been typeset from a TEX/LATEX file prepared by the author.

Downloaded from https://academic.oup.com/mnras/article-abstract/492/3/3803/5700291 by University of Queensland user on 20 April 2020